The Quantum Mixed-Spin Heme State of Barley Peroxidase: A Paradigm for Class III Peroxidases

Barry D. Howes,* Christine B. Schiødt,# Karen G. Welinder,#§ Mario P. Marzocchi,* Jian-Guo Ma,¶ Jun Zhang,¶ John A. Shelnutt,¶ and Giulietta Smulevich*

*Dipartimento di Chimica, Università di Firenze, 50121 Firenze, Italy; #Department of Protein Chemistry, University of Copenhagen, DK-1353, Copenhagen K, Denmark; §Biotechnology Laboratory, Aalborg University, DK-9000 Aalborg, Denmark; and ¶Materials Theory and Computation Department, Sandia National Laboratories, Albuquerque, New Mexico 87185-1349, and Department of Chemistry, The University of New Mexico, Albuquerque, New Mexico 87131, USA

ABSTRACT Electronic absorption and resonance Raman (RR) spectra of the ferric form of barley grain peroxidase (BP 1) at various pH values, at both room temperature and 20 K, are reported, together with electron paramagnetic resonance spectra at 10 K. The ferrous forms and the ferric complex with fluoride have also been studied. A quantum mechanically mixed-spin (QS) state has been identified. The QS heme species coexists with 6- and 5-cHS hemes; the relative populations of these three spin states are found to be dependent on pH and temperature. However, the QS species remains in all cases the dominant heme spin species. Barley peroxidase appears to be further characterized by a splitting of the two vinyl stretching modes, indicating that the vinyl groups are differently conjugated with the porphyrin. An analysis of the currently available spectroscopic data for proteins from all three peroxidase classes suggests that the simultaneous occurrence of the QS heme state as well as the splitting of the two vinyl stretching modes is confined to class III enzymes. The former point is discussed in terms of the possible influences of heme deformations on heme spin state. It is found that moderate saddling alone is probably not enough to cause the QS state, although some saddling may be necessary for the QS state.

INTRODUCTION

Peroxidases are heme-containing enzymes that utilize hydrogen peroxide in one-electron oxidation of different organic substrates. Plant, fungal, and bacterial peroxidases are evolutionarily related and constitute the plant peroxidase superfamily of enzymes, which can be divided into three classes based on structural divergences. Class I peroxidases are intracellular and are of prokaryotic origin. These include chloroplast and cytosol ascorbate peroxidases (APXs), yeast mitrochondrial cytochrome c peroxidase (CCP), and bacterial catalase-peroxidases. Class II comprises extracellular fungal peroxidases such as *Coprinus cinereus* peroxidase (CIP) and lignin-degrading peroxidases. Class III contains a very great variety of secretory plant peroxidases, typified by the classical horseradish peroxidase isoenzyme C (HRPC). In general, within a particular class there is 35–95% sequence identity, whereas between classes the sequence identity is less than 20% (Welinder, 1992).

Barley grain peroxidase isoenzyme 1 (BP 1), a class III peroxidase, has been studied only to a limited extent compared to the model class III peroxidase, HRPC (Dunford and Stillman, 1976; Dunford, 1991). One- and two-dimensional NMR studies have also been made on BP 1 in D_2O potassium phosphate at pH 4.8. The NMR spectra of BP 1 are similar to those obtained for HRPC. However, some differences were found, especially around the heme methyl groups (3-CH_3 and 8-CH_3) (Veitch, 1993). Kinetic studies have shown highly unusual properties of BP 1. In contrast to other plant peroxidases like HRPC, the rate of reaction with hydrogen peroxide is very slow at pH values above 5 and increases as the pH is lowered to 3. In addition, the reaction displays a reversible step (Rasmussen et al., 1993a,b). At acidic pH in the presence of Ca^{2+} ions, the kinetics became biphasic. The slow phase has the properties described above, and the fast phase, which is 100 times faster, behaves like HRPC (Rasmussen et al., 1998).

An explanation of the pH dependence of the BP 1 activity has recently been provided by the x-ray structure of the enzyme (Henriksen et al., 1998). The crystal structure of inactive BP 1 at neutral pH shows that the catalytically important distal histidine has a very unfavorable orientation within the distal pocket (Fig. 1), excluding it from participating in the catalytic cycle. The crystal structure of active BP 1 is unknown but is assumed to resemble that of active peanut and HRPC (Schuller et al., 1996; Gajhede et al., 1997) peroxidases. The importance of the distal histidine position in peroxidase activity has been confirmed by studies on HRPC mutants (Tanaka et al., 1997).

Recently, a comparative study of three class III peroxidases, horseradish peroxidase isoenzyme A2 (HRPA2), soybean peroxidase (SBP), and BP 1, using electronic absorption and resonance Raman (RR) spectroscopy at neutral pH, showed that an unusual heme spin state, a quantum mechanically mixed-spin state (QS), is common to all three proteins at room temperature (Feis et al., 1998). The QS heme state results from the admixture of high-spin (HS) ($S = 5/2$) and intermediate spin (IS) ($S = 3/2$) heme spin states. These observations are consistent with an NMR study of the three HRP isoenzymes: C, A1, and A2 (deRopp et al., 1997). It

Received for publication 5 February 1999 and in final form 15 April 1999.

Address reprint requests to Prof. Giulietta Smulevich, Dipartimento di Chimica, Università di Firenze, Via G. Capponi 9, 50121 Firenze, Italy. Tel: +39-055-2757596; Fax: +39-055-2476961; E-mail: smulev@chim.unifi.it.

0006-3495/99/07/478/15 $2.00

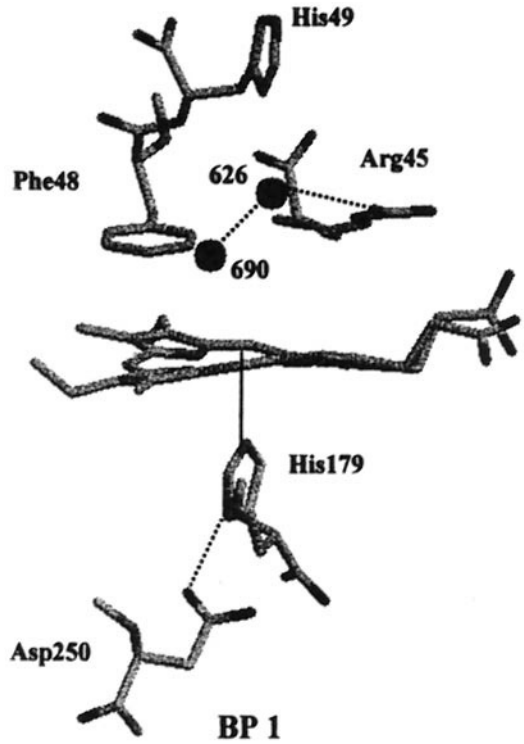

FIGURE 1 Disposition of the amino acid residues in the heme pocket of BP 1, based on the x-ray structure (Henriksen et al., 1998).

was proposed that the three proteins differ in the extent to which a $S < 5/2$ (likely $S = 3/2$) spin state is quantum mechanically admixed with the HS state. The admixture is smallest for HRPC and largest for HRPA2. The QS heme state had previously been observed only rarely in biological systems, e.g., cytochrome c' (Maltempo et al., 1974; Fujii et al., 1995) and HRPA2 and HRPC at low temperature (Maltempo et al., 1979; Smulevich et al., 1991).

In this paper a detailed spectroscopic characterization of BP 1 by RR, electronic absorption, and electron paramagnetic resonance (EPR) at room and low temperature is reported to offer a greater understanding of this unusual heme spin state and its apparent limitation of class III proteins within the plant peroxidase superfamily. In addition, the conformation of the hemes of all of the x-ray crystal structures of peroxidases contained in the Protein Data Bank are analyzed by the normal-coordinate structural decomposition (NSD) method (Jentzen et al., 1997). The possible correlation between the heme deformation and the QS heme spin state is discussed on the basis of the complete body of structural data currently available for the peroxidases.

MATERIALS AND METHODS

Materials

HRPC (Sigma; type VI-A, RZ = 3.1) was used without further purification. BP 1 was purified from barley grain and separated into the glycosylated BP 1a and nonglycosylated BP 1b forms as previously described (Rasmussen et al., 1997). BP 1a and BP 1b give identical spectra and identical enzyme kinetics. The preparation used in the present studies contained 80% BP 1a and 20% BP 1b. The purified protein was stored either as an ammonium sulfate precipitate at 4°C and dialyzed extensively against 1 mM $CaCl_2$ and buffer before use, or as lyophilized protein, which was dissolved in buffer before use. Calcium was present in all buffers to increase peroxidase stability. At pH 4.0 a 50 mM Na citrate, 1 mM $CaCl_2$ buffer was used. Samples at pH 3.3 were prepared by adjusting the pH of pH 4.0 samples by the addition of small amounts of citric acid immediately before use. At pH 6.5 a 0.1 M Na phosphate buffer was used, and a 0.1 M HEPES buffer was used at pH 8.5, both with 1 mM $CaCl_2$ added. Spectra obtained with protein stored by either method or purified from barley grown in different years were identical. The RZ value of the samples after dialysis was 2.9. The enzyme concentrations were determined using an extinction coefficient of 105 mM^{-1} cm^{-1} at 400 nm. An enzyme concentration of ~60 μM was used for Raman excitation in the Soret band, and a concentration of ~300 μM was used for excitation in the visible region. Sample concentrations for low-temperature RR, for both Soret and visible excitation, were ~300 μM. The concentration of the EPR samples was ~100 μM. Single crystals of BP 1 at pH 7.5 were prepared as previously reported (Henriksen et al., 1998) and kindly provided by Dr. A. Henriksen (University of Copenhagen, Denmark).

The ferrous samples were prepared by adding 3 μl of dithionite (20 mg ml^{-1}) to 50 μl of deoxygenated peroxidase solution at pH 6.5. Fluoride complexes were prepared by adding small amounts of solid NaF to BP 1 samples prepared at pH 4.0 and subsequently adjusting the pH by the addition of small quantities of citric acid.

Spectroscopy

The absorption spectra were measured with a Cary 5 spectrophotometer. Room temperature spectra were recorded using a cuvette of 1 mm path length. Low temperature spectra were obtained as previously described (Feis et al., 1994).

RR spectra at room (~15°C) and low temperature and in polarized light were obtained as described elsewhere (Feis et al., 1994; Smulevich et al., 1994a), with excitation from the 413.1-nm and 568.2-nm lines of a Kr^+ ion laser (Coherent; Innova 90/K) and from the 457.9-nm, 496.5-nm, and 514.5-nm lines of an Ar^+ ion laser (Coherent; Innova 90/5). At room temperature, to minimize heating of the protein by the laser beam and to maintain sample integrity for a minimum of 1 h, the sample was cooled (to ~15°C) by a gentle flow of nitrogen gas passed through liquid nitrogen.

The RR spectra of the randomly oriented crystallites were obtained with a Raman microprobe instrument equipped with an Ar^+ ion laser source, a microscope stage, a triple monochrometer, and a CCD detector (Dipartimento di Scienze della Terra, Università di Firenze).

The RR spectra were calibrated to an accuracy of 1 cm^{-1} for intense isolated bands, with indene as the standard for the high-frequency region and indene and CCl_4 for the low-frequency region. Polarized spectra were obtained by inserting a polaroid analyzer between the sample and entrance slit of the monochromator. The depolarization ratios of the bands at 314 and 460 cm^{-1} of CCl_4 were measured to check the reliability of the polarization measurements. The values obtained, 0.73 and 0.00, compared well with the theoretical values of 0.75 and 0.00, respectively. To determine peak intensities and positions, a curve-fitting program was used to simulate experimental spectra, using a Lorentzian lineshape. The following bandwidths (cm^{-1}) were used in the simulations: ν_3 13.5, ν_{11} 11.0, ν_2 12.0, ν_{19} 12.0, ν_{37} 14.0, ν_{10} 11.0, and vinyl ν(C═C) 12.0.

EPR spectra were recorded on a Bruker ESP300 instrument (University of Sussex) equipped with a NMR gaussmeter and a microwave frequency counter. The low-temperature measurements were made using an Oxford Instruments ESR 900 cryostat. The spectra were recorded at 10 K, 9.68 GHz microwave frequency, 1 mW microwave power, and 10 G modulation amplitude.

Normal-coordinate structural decomposition

Jentzen and Shelnutt (Jentzen et al., 1997) have developed a method for classifying and quantifying the out-of-plane and in-plane distortions of the porphyrin macrocycle. In its simplest form, the normal-coordinate structural decomposition (NSD) method uses a linear combination of the six lowest frequency out-of-plane normal coordinates of the macrocycle, one for each out-of-plane D_{4h} symmetry type, to simulate the nonplanar macrocyclic distortion. In most cases, out-of-plane distortions of the macrocycle can be described adequately by summing just these six displacements. Pure displacements along these coordinates correspond to the commonly observed symmetrical deformations seen in x-ray crystal structures. The amounts (in Å) of the saddling (*sad*), ruffling (*ruf*), doming (*dom*), waving [*wav*(*x*) and *wav*(*y*)], and propellering (*pro*) deformation types required to accurately represent the observed out-of-plane distortions of the porphyrin macrocycle are determined for a given structure by the NSD procedure.

RESULTS

Spectroscopy

Room temperature

Electronic absorption spectra of BP 1 at various pH values are shown in Fig. 2. Only minor differences are observed as the pH is raised from 3.3 to 8.5. Between pH 3.3 and pH 6.5, the Soret band blue-shifts from 401 to 398 nm, whereas the porphyrin-to-metal charge transfer band (CT1) upshifts from 638 to 640 nm. The spectra are therefore indicative of high-spin heme. The 1 nm red-shift and the increased extinction coefficient of the pH 8.5 spectrum with respect to pH 6.5 implies slightly more 6-cHS at pH 8.5. However, the Soret maxima are all blue-shifted with respect to that associated with typical HS hemes.

On the basis of the comparative analysis of spectroscopic data for HRPA2, SBP, and BP 1 (Feis et al., 1998), which display different proportions of the QS heme species but similar vinyl conjugation, it was inferred that an increasing presence of the QS species causes an increasing blue-shift of the $\pi \rightarrow \pi^*$ transitions. The blue-shifted Soret maximum for all BP 1 spectra in the pH range 3.3–8.5 are, therefore, clearly indicative of the presence of a QS species in BP 1 at all of the pH values studied. The increased blue-shift of the Soret on passing from pH 3.3 to pH 6.5 is suggestive of an increased proportion of QS at pH 6.5. However, the contrasting red-shift of the CT1 band at pH 6.5 suggests an increased amount of 5-cHS compared to pH 3.3. Comparison with cytochrome *c*′ (cyt *c*′) (Maltempo, 1976) also suggests the presence of a QS heme form in BP 1. No bands characteristic of a low-spin (LS) heme are observed.

Fig. 3 shows the high-frequency region of the RR spectra of BP 1 at various pH values. It appears that at least three sets of core size marker bands are present, corresponding to three different species, which display only small, though significant, changes with pH. Inspection of the ν_3 band gives the clearest indication of the pH-induced changes in the relative populations of the heme spin forms, although the changes noted for the ν_3 band are also reflected in the other modes of the RR spectra. The ν_3 band shows three components at 1481, 1492, and 1503–1504 cm^{-1}. The first two are typical of 6-cHS and 5-cHS heme forms (Choi et al., 1982); however, the band at 1503 cm^{-1} can be interpreted as either 6-cLS or QS. In fact, QS hemes are expected to have RR frequencies close to those of LS hemes because of only partial occupation of the $d_{x^2-y^2}$ orbital (Spiro and Li, 1988). Given the absence of LS forms in the absorption spectrum, the QS form is clearly favored. The highest

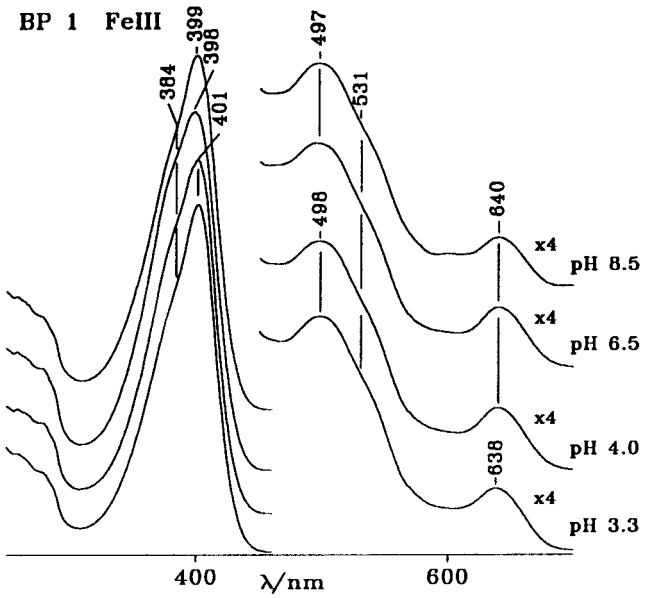

FIGURE 2 Electronic absorption spectra of 340 μM BP 1 at pH 3.3, 4.0, 6.5, and 8.5.

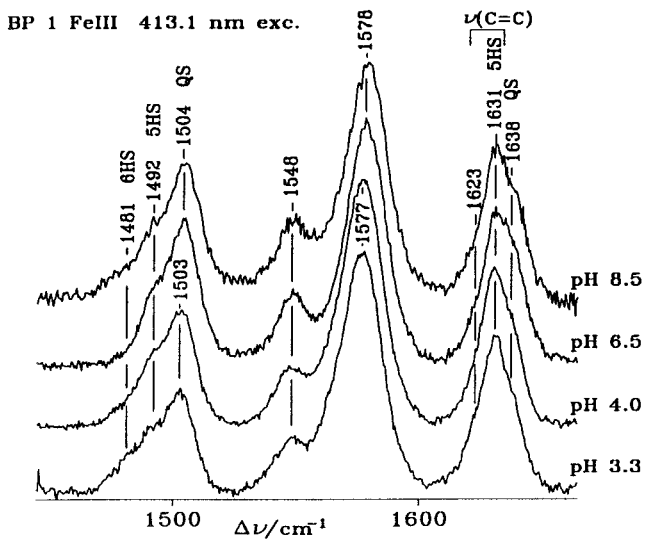

FIGURE 3 Resonance Raman spectra of 65 μM BP 1 at pH 3.3, 4.0, 6.5, and 8.5, recorded with 413.1-nm excitation. Experimental conditions: 5 cm^{-1} resolution; 21s/0.5 cm^{-1} collection interval, 15 mW laser power at the sample (pH 8.5); 25s/0.5 cm^{-1} (pH 6.5), 119s/0.5 cm^{-1} (pH 4.0), and 16s/0.5 cm^{-1} (pH 3.3) collection interval, 25 mW laser power at the sample; 5, 6HS indicate that the bands are due to 5- and 6-cHS hemes, respectively, and QS indicates the band results from the quantum mixed-spin heme.

proportion of the 6-cHS is found at pH 3.3, it is absent at pH 6.5, but it increases slightly again at pH 8.5. The QS heme, which in all cases is the dominant spin form, is at its greatest at pH 6.5. This can be seen not only from the increased relative intensity of this form in the ν_3 band, but also by the 1 cm^{-1} upshift of the ν_3 and the ν_2 bands (1578 cm^{-1}) of the QS form, and the increased relative intensity of the shoulder at 1638 cm^{-1}, corresponding to the ν_{10} mode of the QS heme. The QS ν_{11} mode occurs at an unexpectedly low RR frequency in BP 1, as also previously observed for SBP and HRPA2 (Feis et al., 1998). The origin of this observation, however, remains unclear at present. The bands resulting from the ν_{10} modes of the 5- and 6-cHS are hidden by the vinyl stretching bands. The bands at 1623 and 1631 cm^{-1} are assigned to vinyl stretching. Two vinyl modes, with nearly the same frequencies and relative intensity as BP 1, are also observed in HRPC (Smulevich et al., 1994b), HRPA2, SBP (Feis et al., 1998), and APX (Nissum et al., 1998b). Based on a study of mono- and divinyl hemins (Kalsbeck et al., 1995) and a comparison of APX and CCP data, the higher frequency vinyl band has been assigned to the vinyl in position 2, and the protein matrix has been shown to play an important role in directing the orientation of the vinyl groups of the heme chromophore (Nissum et al., 1998b). In CCP the Met^{172} side chain is in close proximity to vinyl 2, whereas in APX this residue is a serine that imposes a much reduced steric constraint on vinyl 2. The same serine residues are also found at this position and in close proximity to vinyl 2 in HRPC and BP 1.

The changes observed between the RR spectra at various pH values are in complete agreement with those previously described for the electronic absorption spectra. In particular, the absence of a 6-cHS species at pH 6.5 compared to pH 3.3 explains the apparent contradiction in the red-shift of the CT1 band as the pH is raised from 3.3 to 6.5. The absence of the 6-cHS heme at pH 6.5 is expected to blue-shift the Soret but to red-shift the CT1 (Smulevich, 1998).

Extension of the RR analysis (Fig. 4) by excitation at wavelengths in the visible region to enhance the non-totally symmetrical modes, by the use of polarized light to distinguish the bands deriving from modes of different symmetry and by curve-fitting the spectra, has enabled the band frequencies corresponding to all of the core size marker bands to be determined. The absence of any 6-cLS heme is confirmed by the RR spectra obtained with excitation at 568.2 nm. In fact, this wavelength is in resonance with the α band of the 6-cLS heme when present. No enhancement of RR bands due to 6-cLS heme could be observed with respect to the spectrum obtained for 496.5-nm excitation.

The number of RR studies of relevant QS porphyrin systems reported in the literature is very small. The BP 1 core size frequencies (Table 1) do not show close similarity with the reported 5- or 6-cIS model compounds (Teraoka and Kitagawa, 1980). However, the close correspondence of the BP 1 frequencies with those of cyt c', isolated from various bacteria (Strekas and Spiro, 1974; Othman et al., 1996), known to be 5-cQS, suggests an assignment of BP 1 as 5-cQS. Such an assignment is also indicated by the structure of BP 1 (Henriksen et al., 1998), which shows that the closest water molecule is 5.7 Å from the Fe atom. An important observation in this regard is that the RR spectra of randomly oriented crystallites at pH 7.5 taken with 497.5-nm excitation closely resemble those in solution (Fig. 4), allowing a direct comparison of the spectroscopic results with those of the crystal structures between pH 5.5 and 8.5 (Henriksen et al., 1998).

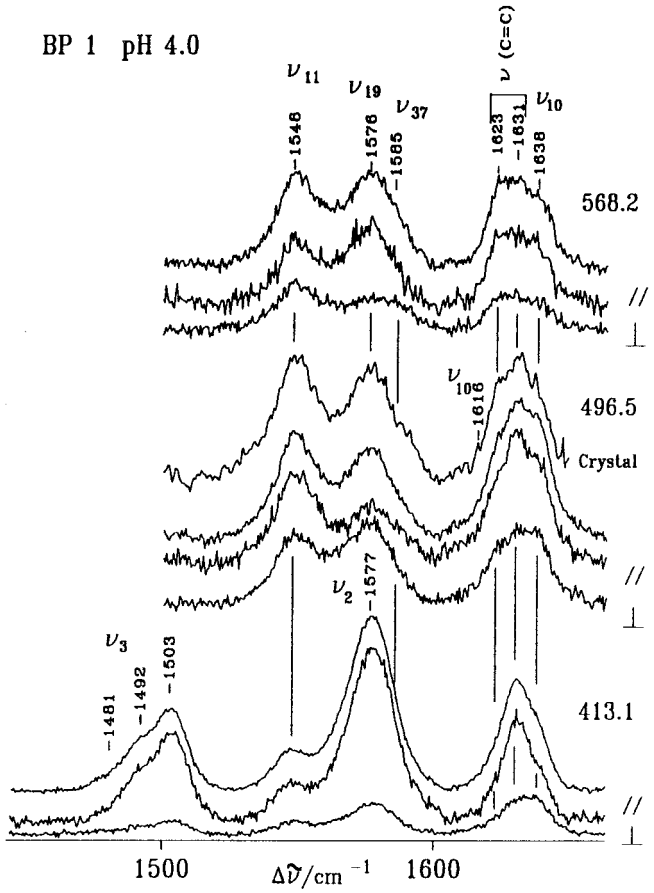

FIGURE 4 Resonance Raman spectra of BP 1 recorded in polarized light with excitation at 413.1, 496.5, and 568.2 nm at pH 4.0. Experimental conditions: 5 cm^{-1} resolution; (413.1 nm) concentration 65 μM, 20s/0.5 cm^{-1} (parallel), and 40s/0.5 cm^{-1} (perpendicular) collection interval, 25 mW laser power at the sample; (496.5 nm) concentration 280 μM, 36s/0.5 cm^{-1} collection interval, 60 mW laser power at the sample; (568.2 nm) concentration 280 μM, 40s/0.5 cm^{-1} collection interval, 65 mW laser power at the sample. For comparison the RR spectrum, for 496.5-nm excitation, of randomly oriented crystallites at pH 7.5 is also shown. The spectrum is an average of 72 spectra with accumulation times of 120 s each. Experimental conditions: 5 cm^{-1} resolution; 2.5 mW laser power at the sample with a defocused beam.

The absorption spectrum at pH 3.5 of the BP 1 fluoride adduct (Fig. 5, *right*) is very similar to that obtained for the fluoride complex of HRPC (Keilin and Hartree, 1951), HRPA2 (Feis et al., 1998), and SBP (Nissum et al., 1998a), being characteristic of a 6-cHS heme. The RR bands of the fluoride adduct at pH 3.5 (Fig. 5, *left*) at 1479 (ν_3), 1566

TABLE 1 Resonance Raman frequencies (cm^{-1}) of the heme states observed for BP 1 between pH 3.3 and 8.5*

	Room temperature			
Mode	6-cHS	5-cHS	QS	20 K QS[#]
ν_3	1481	1492	1504[#]	1515
ν_2[§]	1563	1572	1579	1588
ν_{11}		1555	1548	1555
ν_{19}		1567	1576	1587
ν_{37}[##]		1585		
ν_4[##]		1373		1376
ν(C═C)[##]		1623[¶]		[‖]
ν(C═C)[##]		1631		1634
ν_{10}	1616	1634**	1638	1648

*The listed RR bands and their frequencies are those determined by curve-fitting the pH 4 spectra.
[#]Frequencies determined from the pH 6.5 spectra.
[§]The frequency of the room temperature ν_2 band maximum is 1577 cm^{-1} (pH 3.3 and 4.0) and 1578 (pH 6.5 and 8.5) (Figs. 3 and 4).
[¶]This band could not be accurately positioned.
[‖]The weakness of the band makes it difficult to position.
**Because of overlap with the vinyl modes, this band could not be accurately positioned.
[##]The frequencies for the various heme states are not distinguishable.

(ν_2), and 1608 (ν_{10}) cm^{-1} are assigned to the 6-cHS heme species of the F^- complex, and the asymmetrical band centered at 1630 cm^{-1} is assigned to the vinyl stretching modes. A very small amount of QS heme remains, implying that F^- does not bind completely to BP 1. A slightly higher proportion of the QS form remains at pH 5.4 (data not shown), indicating that F^- binding decreases at the higher pH. This result is in agreement with kinetic studies of fluoride binding, which give a K_d of 12 ± 3 mM at pH 3.3 and >1.6 M at pH 5.4 (Rasmussen et al., 1998). It is noted that the band at 1577 cm^{-1} is relatively intense, probably because of the overlap of the QS ν_2 mode and the ν_{37} mode of the 6-cHS state of the fluoride complex, expected at ~1585 cm^{-1}, by analogy with the met-hemoglobin fluoride adduct (Choi et al., 1982).

Electronic absorption and RR spectra of ferrous BP 1 at pH 6.5 are shown in Fig. 6. The absorption spectrum is similar to the spectra obtained for other peroxidases, e.g., HRP-C (Keilin and Hartree, 1951), CCP (Conroy et al., 1978), and CIP (Smulevich et al., 1994a), with the Soret band at 437 nm and the Q bands at 557 and 585 nm. The high-frequency RR spectrum has core size marker band frequencies very similar to those of HRPC, CCP(MI), and CIP (Smulevich et al., 1994a). Both the absorption and high-frequency RR spectra are characteristic of a 5-cHS heme. An intense vinyl band is observed at 1624 cm^{-1}. However, the band is broad and asymmetrical, indicating that the second weak vinyl mode is placed at slightly lower frequency at ~1620 cm^{-1} in the ferrous state. This behavior is similar to that of ferrous HRPC (Smulevich et al., 1994a), SBP (Nissum et al., 1998a), and APX (Nissum et al., 1998b).

The low-frequency RR spectrum is also shown in Fig. 6 *a*. The prime interest in this region for 5 coordinate heme proteins is the presence of a strong band due to the iron-imidazole stretching mode, ν(Fe-Im), which occurs in the range 200–250 cm^{-1}. The polar hydrogen bond between the N_δ atom of the imidazole fifth ligand and the oxygen atom of the aspartate carboxylate group, characteristic of peroxidases, gives the proximal ligand imidazolate character. The consequence of this effect is to strengthen the Fe-imidazole bond and to give a higher frequency of the associated vibrational mode (only visible in the ferrous oxidation state) compared to other heme proteins. Therefore, because of its sensitivity to the Fe-Im bond strength, the ν(Fe-Im) stretching mode is a useful probe of the strength of the hydrogen bond between the conserved proximal histidine and aspartate residues. The intense band observed at 244 cm^{-1} in HRPC has been assigned to the ν(Fe-Im) stretching mode on the basis of the ^{54}Fe isotopic shift (Teraoka and Kitagawa, 1981). By analogy, the strong band observed at 237 cm^{-1} in BP 1 is assigned to the ν(Fe-Im) stretching mode. Raising the pH of reduced BP 1 from 6.5 to 10 caused no observable shift of the 237 cm^{-1} band. The bands at 311, 348, 375, and 407 cm^{-1} are assigned to γ_6, ν_8, the bending mode of the propionyl groups, and the bending modes of the vinyl groups, respectively.

Low temperature

Comparison of the room temperature and 20 K absorption spectra of BP 1 at various pH (Figs. 2 and 7) shows that significant changes are induced as the temperature is lowered. The Soret bands are red-shifted at 20 K, and this effect is particularly pronounced in the pH 6.5 spectrum (it is noted that in the room-temperature, pH 6.5 spectrum, the Soret band is blue-shifted with respect to the pH 4.0 spectrum). The CT1 bands, placed at 640 nm at room temperature, are strongly blue-shifted at 20 K, being positioned at 634 nm and 632 nm at pH 4.0 and 6.5, respectively. Hence the effect is again particularly clear in the pH 6.5 spectrum.

The low-temperature absorption spectrum of HRPC is shown for comparative purposes in Fig. 7. The spectrum in the 450–700-nm region is the same as that previously reported for HRP-C at pH 6 and measured at 80 K (Tamura, 1971; Smulevich et al., 1999). More marked changes are observed in the absorption spectrum of HRPC than in the absorption spectrum of BP 1 as the temperature is lowered. The pronounced bands at 567 nm and 534 nm and the Soret shoulder at 418 nm (not present in BP 1) clearly imply a significant proportion of LS in HRPC at 20 K, which is not present at room temperature (Dunford and Stillman, 1976). A further species, characterized by bands in the visible at 491 nm and 634 nm, appears to be present and is consistent with a HS or QS heme. The latter is strongly suggested by its close similarity to the spectrum of cyt *c′* at 80 K (Maltempo, 1976), which is characterized by a QS heme state only. This result is in agreement with the previous low-temperature RR and EPR spectra of HRPC, which indicate

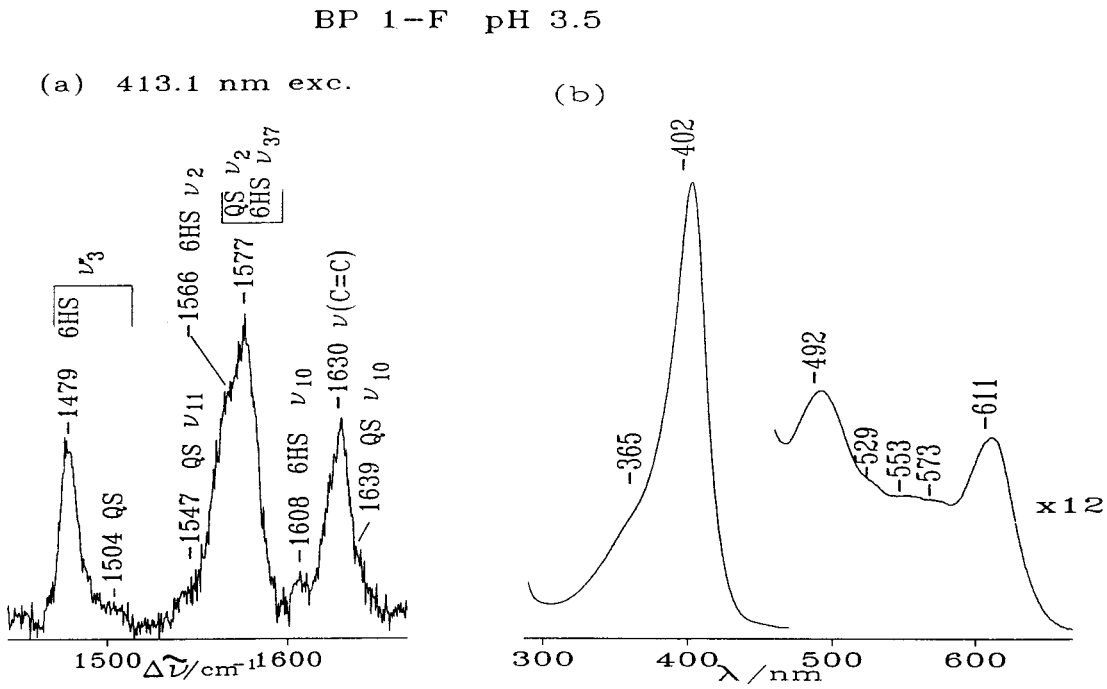

FIGURE 5 (*a*) Resonance Raman spectra of 100 μM BP 1 fluoride adduct at pH 3.5 recorded with 413.1-nm excitation. Experimental conditions: 5 cm^{-1} resolution, 6s/0.5 cm^{-1} collection interval, 25 mW laser power at the sample. 6HS indicates that the bands are due to 6-cHS heme of the fluoride adduct, and QS indicates that the band results from the quantum mixed-spin heme. (*b*) Absorption spectrum of the BP 1 fluoride adduct at pH 3.5.

the presence of LS and QS species (Schonbaum, 1973; Smulevich et al., 1991).

Considerable changes are also observed in the RR spectra as the temperature is lowered (Figs. 3 and 8). It is immediately apparent that the core size marker bands of the QS species are upshifted by ~10 cm^{-1} at 20 K (Table 1). The high-frequency vinyl stretching mode is also upshifted by 4 cm^{-1} at 20 K. Only the highest frequency vinyl mode is marked, as the second one is too weak to be clearly positioned. In HRPC at 10 K, only the highest frequency mode was upshifted by ~3 cm^{-1}, indicating that the conformation of only one vinyl group is sensitive to changes in the temperature (Smulevich et al., 1991). The spectra shown in Fig. 8 for excitation at 413.1 and 514.5 nm indicate a marked increase in the population of the QS heme species at 20 K. This is clearly seen for excitation at 413.1 nm at pH 4.0; for example, the ν_3 band is dominated by the QS heme form, and only a little HS heme remains at ~1492 cm^{-1}. The HS ν_{10} band is expected to be weak and hidden under the more intense vinyl modes. The conversion to the QS form is even more complete at pH 6.5. This can be seen by the absence of the HS ν_3 band at ~1492 cm^{-1} and the slight upshift of the core size marker band frequencies at pH 6.5. Therefore, the frequencies observed at pH 6.5, 20 K (Table 1) characterize a single heme spin state, that of the QS heme at 20 K. The room-temperature assignment of the band at 1547 cm^{-1} to the ν_{11} mode of the QS heme, at an unexpectedly low frequency, is confirmed by its frequency at 20 K (1555 cm^{-1}).

At pH 4.0 it was found that high enzyme concentrations (~300 μM) partially inhibited conversion from HS to the QS heme (data not shown). It is also worth noting that the relative intensity of the ν_4 band with respect to the other core size marker bands, for Soret excitation, is considerably reduced at 20 K (data not shown). This is clearly seen for the pH 6.5 spectrum and the ν_3 band in particular. This behavior was also evident at room temperature, but it becomes particularly marked at low temperature.

The EPR spectra of BP 1 (Fig. 9) show that significant changes are induced as the pH is raised from 4.0 to 6.5. The spectral form of the pH 4.0 spectrum indicates that it is a superposition of HS ($g_\perp$ = 5.84) and QS ($g_\perp$ = 5.66) hemes. Although, in principle, any species with $4 < g_\perp < 6$ and $g_\parallel = 2$ should be denoted as QS, a $g_\perp$ = 5.84 signal is typically regarded as being essentially HS (Maltempo et al., 1979). However, the $g_\perp$ = 5.66 species clearly has a significant contribution of the intermediate spin state and, necessarily, must be defined as resulting from a QS state. The feature at g = 4.3 is due to a small amount of nonheme rhombic iron commonly seen in the EPR spectra of proteins (Blumberg et al., 1968). It is noted that the $g_\perp$ values of the QS for HRPC and HRPA2, at pH 7 and 5 K, are ~5.0 and ~5.6, respectively (Maltempo et al., 1979). The pH 6.5 spectrum retains a small proportion of the signals at $g_\perp$ = 5.84 and 5.66 but is dominated by an apparently rhombic EPR signal (g = 5.36, 3.75, 1.93). To counter this interpretation of the pH 6.5 spectrum, the absorption feature at g = 3.75 for a typical rhombic EPR signal is expected to extend below the baseline in a more pronounced way than observed and may indicate the presence of two axial QS species rather than a rhombic species. However, given that large linewidths have been associated with QS systems (Mal-

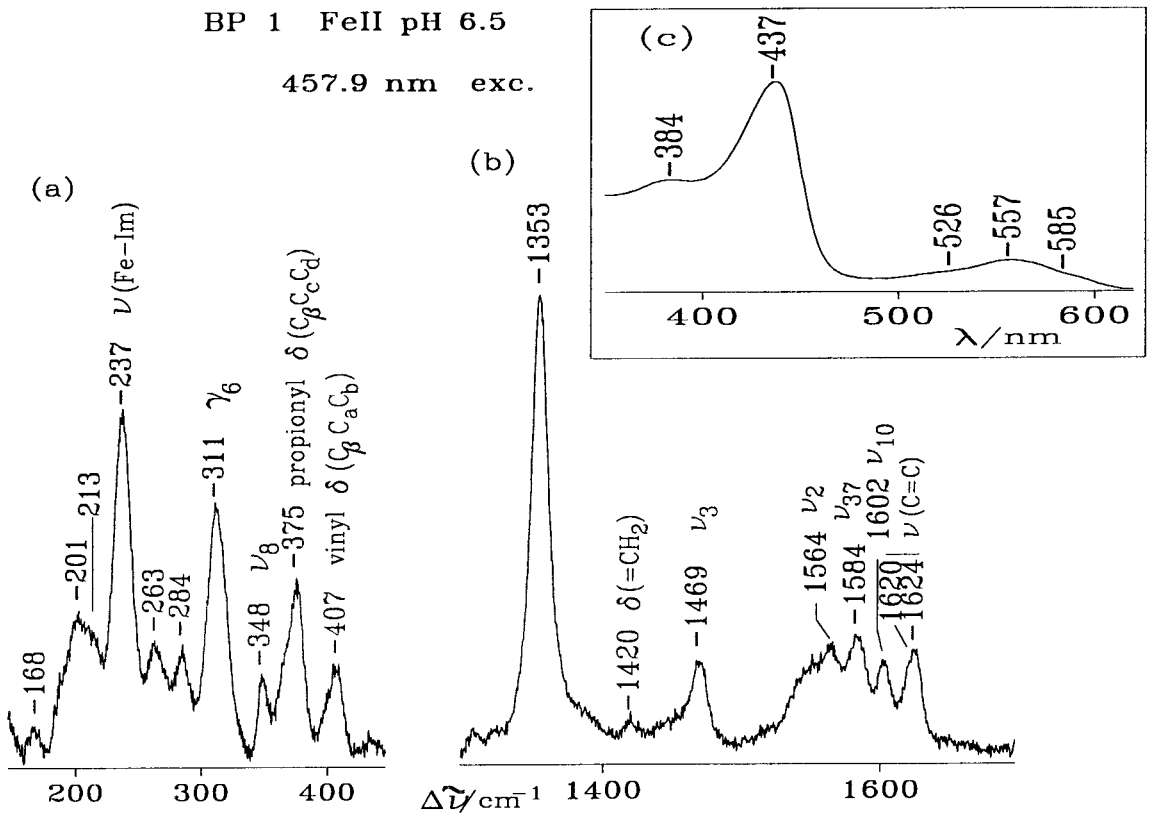

FIGURE 6 Resonance Raman and absorption spectra of ferrous BP 1. Resonance Raman spectra of 150 μM ferrous BP 1 at pH 6.5 with 457.9-nm excitation at low frequency (*a*) (experimental conditions: 5 cm^{-1} resolution, 16s/0.5 cm^{-1} collection interval, 25 mW laser power at the sample) and high frequency (*b*) (experimental conditions: 5 cm^{-1} resolution, 6s/0.5 cm^{-1} collection interval, 25 mW laser power at the sample). The low-frequency RR spectrum (*a*) is multiplied by a factor of 4 with respect to the high-frequency spectrum (*b*). (*c*) Absorption spectrum of 100 μM ferrous BP 1 at pH 6.5.

tempo et al., 1974; Fujii et al., 1995), it is possible that this unusual feature is a consequence of the linewidth. The broad feature at $g = 1.93$ has also previously been observed for QS systems (Maltempo et al., 1974; Leigh et al., 1975). Although it is considered to be unlikely, the possibility that power saturation effects distort the lineshape to some extent cannot be completely excluded. A power and temperature dependency study would be necessary to demonstrate conclusively that the signals at $g = 5.36$ and 3.75 result from the same electronic transitions. A weak low-spin heme signal ($g = 3.38$) is present at pH 4. No evidence was found for low-spin heme signals at pH 6.5.

Normal-coordinate structural analysis

The distortions of the hemes of all of the x-ray crystal structures of the peroxidases contained in the Protein Data Bank were analyzed by normal-coordinate structural decomposition (NSD). The NSD computational method is described completely elsewhere (Jentzen et al., 1997, 1998). The NSD results are given in Table 2 and Figs. 10–12. The NSD method provides a description of the conformation of the heme macrocycle in terms of equivalent displacements along the normal coordinates. For the protein crystal structures, typically only the deformations along the lowest-frequency normal mode of each out-of-plane symmetry type is statistically significant and thus is given in Table 2. Nonetheless, the linear combination of only these six deformations usually provides an adequate representation of the heme structure. That is, most of the heme distortion typically occurs along these six most deformable normal coordinates.

Fig. 10 illustrates the out-of-plane deformations along the normal coordinates that make up the observed distortions of the hemes in the x-ray crystal structures of the native peroxidase proteins. The NSD results for the structurally unrelated myeloperoxidase is also illustrated. Fig. 11 compares the distortions of the hemes in the cytochrome *c* peroxidase mutants and wild type. The x-ray crystal data are taken from the Protein Data Bank (Abola et al., 1987, 1997).

DISCUSSION

Heme spin states

A combined analysis of room temperature electronic absorption and RR spectra of ferric BP 1 between pH 3.3 and 8.5 indicates that it is a mixture of three heme spin forms: 6-cHS, 5-cHS, and quantum mechanically mixed-spin (QS), the QS heme state constituting the dominant species. Low-

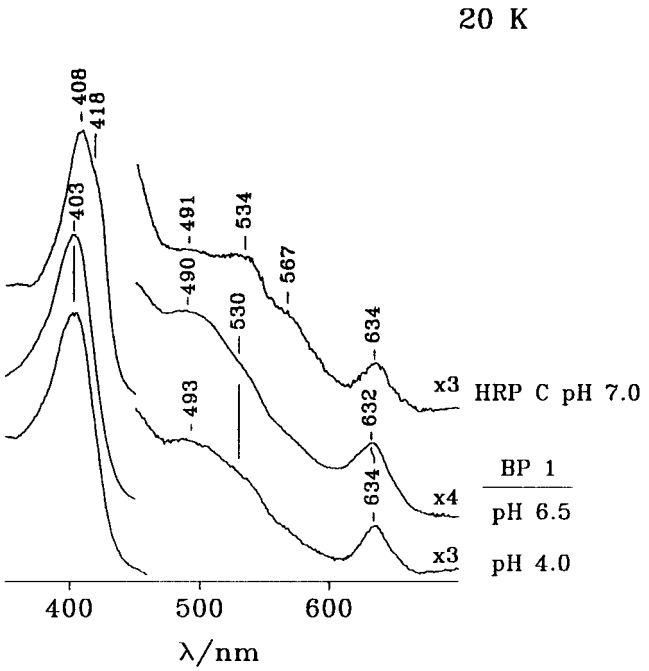

FIGURE 7 Absorption spectra at 20 K of BP 1 at pH 4.0 and 6.5 and HRPC at pH 7.0.

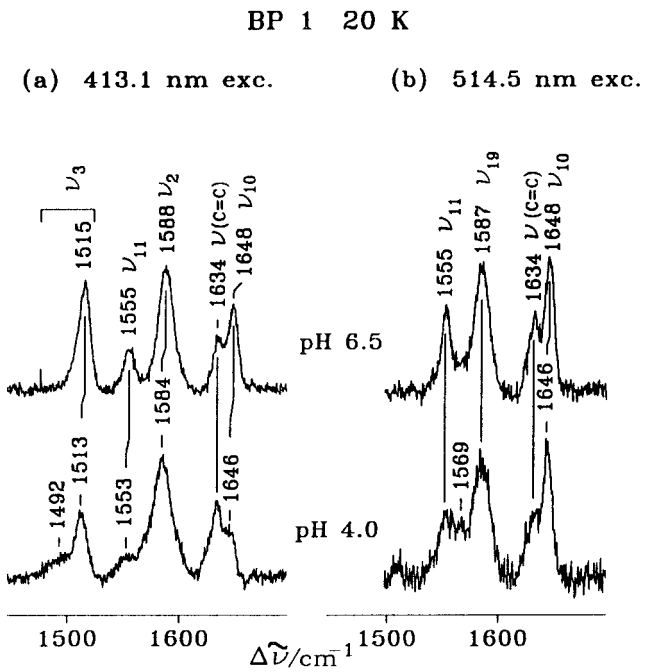

FIGURE 8 Resonance Raman spectra at 20 K of 300 μM BP 1 at pH 4.0 and 6.5. (*a*) 413.1-nm excitation. Experimental conditions: 5 cm^{-1} resolution; 10s/0.5 cm^{-1} (pH 6.5), 8s/0.5 cm^{-1} (pH 4.0) collection interval; 15 mW laser power at the sample. (*b*) 514.5-nm excitation. Experimental conditions: 5 cm^{-1} resolution; 20s/0.5 cm^{-1} (pH 6.5) 9s/0.5 cm^{-1} (pH 4.0) collection interval; 70 mW laser power at the sample.

temperature electronic absorption, RR, and EPR measurements have provided further support for the presence of the QS heme state in BP 1, indicating that BP 1 is a mixture of HS and QS heme forms in thermal equilibrium. The QS state reflects a quantum mechanical admixture of intermediate ($S = 3/2$) and high ($S = 5/2$) spin states and is very unusual in biological systems. It has been found to be a common feature of cytochrome *c′* from various bacterial sources at neutral pH (Fujii et al., 1995; Othman et al., 1996). Within the peroxidase superfamily it has been observed thus far only in class III peroxidases. HRPC displays a clear QS heme spin form only at low temperature (Maltempo et al., 1979; Smulevich et al., 1991), but recently on the basis of NMR data the presence of a small proportion of an IS heme state admixed with the HS state has been observed at room temperature (deRopp et al., 1997). Interestingly, the RR spectra revealed the presence of anomalously higher frequency core size marker bands than those normally observed for 5-c HS and 6-c HS hemes in model compounds (Smulevich et al., 1994b). HRPA2, BP 1, and SBP exhibit a QS heme species at room temperature as one element of a thermal mixture of spin states (Feis et al., 1998). However, BP 1 displays a considerably enhanced proportion of QS heme at low temperature. The observation of the QS heme state only in peroxidases of class III is rather striking and will be considered further in the following section.

The observed ν(Fe-Im) stretching frequency for ferrous BP 1 at pH 6.5 (237 cm^{-1}) is downshifted by 9 and 7 cm^{-1} with respect to CCP and HRPC, respectively, at pH 7 (Teraoka and Kitagawa, 1981; Smulevich et al., 1988, 1996). This indicates a longer Fe-Im bond in BP 1 due to a less imidazolate character of the proximal ligand in BP 1. However, this conflicts with the ferric structural data, which show the Fe-ligand distances for BP 1 (Henriksen et al., 1998), CCP (Wang et al., 1990), and HRPC (Gajhede et al., 1997) to be 2.14 Å, 2.08 Å, and 2.19 Å, respectively. Furthermore, the proximal His-Asp distances are 2.90 Å,

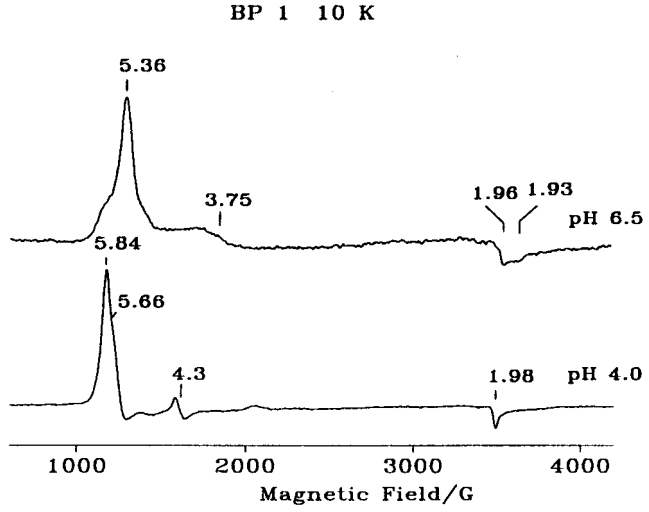

FIGURE 9 EPR spectra of 100 μM BP 1 at pH 4.0 and 6.5. Recording conditions: temperature 10 K, microwave frequency 9.68 GHz, microwave power 1 mW, modulation amplitude 10 G.

TABLE 2 Normal-coordinate structural decomposition of the heme groups of classes I, II, and III peroxidases and mutants, along with several structural parameters

PDB code	Peroxidase		Fe displ. (Å)	Out-of-plane-displacements (Å)							Fe-N*pyr* (Å)	Fe-N*lig* (Å)	Fe-H_2O (Å)	Dihedral angle (°)§
				Total*	*sad*#	*ruf*#	*Dom*#	*wav(x)*#	*wav(y)*#	*pro*#				
Class I														
2CYP	CCP		−0.135	0.725	−0.622	−0.24	0.014	−0.183	−0.049	0.007	2.00	1.95	2.40	−82.11
1CCP	CCPMI		−0.219	0.787	−0.701	−0.238	0.032	−0.164	−0.070	−0.008	2.00	2.08	2.65	−78.09
1CCA	CCPMKT		−0.223	0.657	−0.543	−0.230	−0.089	−0.177	−0.094	−0.010	2.07	2.01	2.17	−83.07
1APX	APX	Hem A	−0.149	0.940	−0.815	−0.133	−0.230	−0.247	−0.025	0.178	2.03	2.16	2.74	−94.56
		Hem B	−0.149	0.807	−0.665	−0.257	−0.241	−0.102	−0.189	0.075	2.04	2.18	3.09	−94.59
		Hem C	−0.115	0.693	−0.573	−0.159	−0.023	−0.059	−0.254	0.052	2.03	2.20	3.12	−90.08
		Hem D	−0.105	0.927	−0.874	−0.168	−0.024	−0.050	−0.151	0.009	2.03	2.20	2.62	−85.95
2PCB	CCP-Cytc	Hem A	−0.270	0.904	−0.856	0.024	0.013	0.073	−0.055	−0.025	2.02	1.94	3.18	−90.88
		Hem C	−0.283	0.811	−0.537	−0.379	0.177	−0.247	−0.131	−0.030	2.02	2.14	2.49	−66.97
2PCC	CCP-Cytc	Hem A	−0.270	0.661	−0.499	−0.247	−0.035	−0.277	−0.030	−0.047	2.02	1.91	2.39(SO_4)¶	−83.51
		Hem C	−0.132	0.764	−0.609	−0.383	−0.160	−0.118	0.013	−0.045	2.01	2.12	2.09(SO_4)¶	−85.76
CCPMKT mutants														
1CCB	D235E		−0.112	0.796	−0.706	−0.314	0.062	−0.118	−0.068	−0.035	2.06	1.99	2.31	−91.5
1CCC	D235A		−0.063	0.824	−0.670	−0.393	−0.030	−0.151	−0.092	−0.003	2.06	2.00	1.86	−78.88
1CCE	H175G		0.028	0.708	−0.541	−0.328	0.104	−0.088	−0.133	0.036	2.06	2.01	2.02(Tyr)¶	−79.01
1CCG	H175G		−0.232	0.667	−0.614	−0.191	−0.048	−0.060	−0.087	−0.003	2.05	2.00	1.99	−85.55
1CMP	W191G		0.019	0.686	−0.499	−0.398	0.011	−0.142	0.006	0.011	2.07	2.00	1.89	−84.36
1CMQ	W191G		−0.048	0.680	−0.476	−0.377	−0.066	−0.057	0.089	0.030	2.06	1.98	2.14	−80.1
1CMT	W191G		0.009	0.691	−0.497	−0.410	0.008	−0.120	0.000	0.004	2.07	2.02	2.01	−89.89
1AA4	W191G		−0.002	0.637	−0.418	−0.375	0.060	−0.173	−0.038	−0.013	2.07	1.98	1.98	−86.94
1AC4	W191G		−0.059	0.641	−0.473	−0.348	0.010	−0.125	0.047	0.041	2.06	2.00	2.02	−79.52
1AC8	W191G		−0.010	0.684	−0.470	−0.380	0.007	−0.181	−0.038	−0.013	2.07	2.00	1.95	−91.36
1AEB‖	W191G		−0.010	0.678	−0.466	−0.375	0.009	−0.181	−0.039	−0.008	2.07	2.00	1.95	−91.58
1AEE	W191G		−0.014	0.710	−0.539	−0.389	−0.026	−0.094	0.008	−0.012	2.07	2.00	2.36	−88.64
1AEN**	W191G		−0.059	0.641	−0.473	−0.348	0.010	−0.125	0.047	0.041	2.06	2.00	2.02	−79.52
1AES	W191G		−0.031	0.659	−0.549	−0.217	−0.108	−0.145	−0.057	−0.041	2.06	1.99	2.02	−92.35
1AET	W191G		−0.023	0.668	−0.479	−0.384	−0.031	−0.154	0.088	0.000	2.07	2.01	1.92	−82.65
1AEV	W191G		−0.093	0.599	−0.495	−0.243	0.007	−0.099	−0.087	0.010	2.07	2.00	1.96	−84.82
1RYC	W191G		−0.015	0.594	−0.478	−0.218	0.020	−0.139	0.010	−0.002	2.07	2.00	2.02	−85.87
1CMU	W191G, D235N		−0.051	0.777	−0.668	−0.314	−0.007	−0.022	−0.095	−0.020	2.07	2.05	1.95	−76.6
1CCJ	F202G		−0.082	0.566	−0.499	−0.137	−0.004	−0.158	−0.032	−0.004	2.07	2.00	2.22	−83.95
3CCX	T52I, A147Y, D152G		−0.338	0.749	−0.699	−0.184	−0.054	−0.132	0	−0.038	2.07	2.02	3.28	−84.28
1CCI	T53I, F202G, D152G		−0.009	0.487	−0.316	−0.180	0.010	0.043	−0.077	−0.036	2.07	1.99	1.76	−89.21
4CCX	T53I, A147M, D152G		−0.215	0.765	−0.617	−0.278	−0.102	−0.222	−0.109	0.013	2.07	2.01	2.06	−81.40
CCPMI mutants														
1CPD	W191G		0.005	0.872	−0.608	−0.427	0.107	−0.013	0.039	−0.218	2.02	2.10	2.23	−89.17
1CPE	W191G		−0.013	0.916	−0.586	−0.483	0.033	−0.172	−0.142	0.063	1.98	2.05	1.88	−62.67
1CPF	W191G		−0.049	0.882	−0.622	−0.470	−0.048	−0.122	−0.054	−0.148	1.99	2.07	2.40	−90.73
1CPG	W191Q		−0.003	0.936	−0.618	−0.401	0.059	−0.146	−0.136	0.115	1.93	2.04	1.90	−77.83
1CYF	C128A, A193C		−0.065	0.768	−0.311	−0.097	−0.029	−0.113	−0.266	−0.184	1.99	2.13	1.80	−80.92
1DCC	W191F		−0.143	0.828	−0.574	−0.365	−0.074	−0.112	−0.129	0.110	1.98	2.11	1.81(O_2)¶	−70.53
2CCP	D235N		−0.012	0.827	−0.712	−0.296	−0.068	−0.130	−0.061	−0.005	1.97	2.01	2.03	−82.89
2CEP	M230I		−0.256	0.719	−0.606	−0.201	0.036	−0.191	−0.097	0.007	2.00	2.17	2.59	−81.10
3CCP	W191F		−0.183	0.840	−0.658	−0.444	0.014	−0.164	−0.095	−0.019	2.02	2.09	2.54	−79.75
4CCP	W51F		−0.179	0.827	−0.712	−0.296	−0.068	−0.130	−0.061	−0.005	2.04	2.10	2.59	−75.93
5CCP	H52L		−0.267	0.946	−0.758	−0.193	−0.171	−0.279	−0.053	−0.117	2.01	2.13	2.89	−70.33
6CCP	R48K		−0.229	0.712	−0.656	−0.153	0.003	−0.150	−0.043	−0.018	2.02	2.09	4.53	−79.26
7CCP	R48L		−0.376	0.783	−0.681	−0.211	0.017	−0.221	−0.064	0.006	2.05	2.04	2.84	−72.47

*Total distortions of the x-ray structure equal to the square root of the sum of squares of the displacements from the mean plane for the 24 atoms of the macrocycle.

#The *ruf* deformation has the pyrrole planes rotated about the Fe-N bonds. In the *sad* deformation, adjacent pyrroles tilt up and down about an axis perpendicular to the Fe-N bond. In the *dom* deformation, all of the pyrroles tilt in the same sense. For the *x*- and *y*-*wav* deformations, two opposite pyrroles rotate, keeping their planes parallel, while one of the other two pyrroles tilt up and the other tilts down. In the *pro* deformation, the pyrroles are all rotated about the Fe-N bond in the same sense as a propeller. These macrocycle deformations are illustrated in Ma et al. (1998b) and Shelnutt et al. (1998).

§The C_α-$N_{pyrrole}$_Fe-N_{ligand} dihedral angle.

¶The closest group to the central Fe.

‖The structures of the W191G mutants 1AED, 1AEF, 1AEG, 1AEH, 1AEJ, 1AEK, 1AEM, 1AEQ are identical to 1 AEB.

**The structures of the W191G mutants 1AEO and 1AEU are identical to 1AEN.

TABLE 2 Continued

PDB code	Peroxidase		Fe displ. (Å)	Out-of-plane-displacements (Å)							Fe-N*pyr* (Å)	Fe-N*lig* (Å)	Fe-H_2O (Å)	Dihedral angle (°)§
				Total*	*sad*#	*ruf*#	*Dom*#	*wav(x)*#	*wav(y)*#	*pro*#				
Class II														
1ARP	ARP		−0.131	1.148	−0.905	−0.659	−0.18	−0.028	−0.146	−0.057	1.97	2.1	2.96	−84.62
1ARU	ARP-CN		−0.100	1.209	−0.954	−0.695	−0.201	−0.012	−0.083	−0.074	1.98	2.13	1.96	−84.18
1ARV	ARP-CN		−0.101	1.239	−0.971	−0.723	−0.219	−0.061	−0.042	−0.091	1.96	2.12	2.03	−82.85
1ARW	ARP-CN		−0.112	1.281	−1.003	−0.723	−0.289	−0.127	−0.034	−0.072	1.96	2.09	2.02	−83.5
1ARX	ARP-I_3		−0.257	1.070	−0.915	−0.433	−0.250	−0.044	−0.168	−0.04	1.96	2.09	3.25	−88.98
1ARY	ARP-I_3		−0.260	0.899	−0.776	−0.353	−0.244	−0.059	−0.066	−0.069	1.97	2.13	3.29	−86.09
1GZA	ARP		−0.318	1.234	−1.076	−0.471	−0.337	−0.148	−0.041	−0.068	1.97	2.11	3.74	−82.61
1GZB	ARP		−0.320	1.346	−1.103	−0.634	−0.369	−0.205	−0.019	−0.080	1.97	2.14	3.9	−81.97
1LGA	LIP	Hem A	−0.155	0.617	−0.517	−0.075	−0.226	−0.175	0.027	−0.064	1.97	2.15	2.73	−91.16
		Hem B	−0.197	0.559	−0.481	−0.100	−0.156	−0.160	0.047	−0.004	1.95	2.19	2.71	−91.30
1QPA	LIP	Hem A	−0.066	0.770	−0.546	−0.351	0.051	−0.264	−0.093	−0.075	2.03	2.13	2.04	−86.58
		Hem B	−0.078	0.777	−0.546	−0.448	−0.035	−0.18	0.039	−0.039	1.99	2.26	2.09	−77.47
1LLP	LIPH2		−0.106	0.676	−0.579	−0.083	−0.057	−0.240	0.067	0.016	2.06	2.15	2.27	−88.00
1MNP	MnP		−0.153	0.729	−0.631	−0.277	−0.163	−0.070	−0.066	−0.014	2.01	2.28	2.8	−88.92
1MN1	MnP-D179N		−0.192	0.732	−0.604	−0.284	−0.174	−0.126	−0.153	−0.031	2.01	2.27	2.79	−90.97
1MN2	MnP-E35Q, D179N		−0.093	0.593	−0.487	−0.281	−0.119	−0.085	−0.04	−0.024	2.03	2.36	2.66	−88.92
Class III														
1ATJ	HRPC		−0.168	0.916	−0.871	−0.084	−0.067	−0.141	−0.208	0.000	1.98	2.19	3.20	−85.29
1BGP	BP 1		−0.214	1.194	−1.144	−0.265	−0.085	−0.033	−0.14	−0.023	1.97	2.14	5.44	−84.88
1SCH	PNP	Hem A	−0.125	1.174	−0.945	−0.586	−0.062	−0.226	−0.202	−0.072	1.96	2.10	3.10	−82.73
		Hem B	−0.106	1.484	−1.347	−0.533	−0.015	−0.058	−0.218	0.014	1.98	2.13	3.80	−84.59
2ATJ	HRPC-BHA	Hem A	−0.142	0.743	−0.691	0.040	0.051	−0.142	−0.188	0.016	2.00	2.21	2.63	−88.66
		Hem B	−0.142	0.743	−0.691	0.040	0.051	−0.141	−0.188	0.016	2.00	2.21	2.63	−88.64

2.89 Å, and 2.76 Å, respectively. Although these differences are close to the limits detectable at the resolution of the various structures, there is no correlation between the ferrous RR data and the ferric structural data in these cases. Moreover, in the present case, as the Fe-Im stretch is observed only in the 5-cHS ferrous heme proteins and not in the ferric state, it would be difficult to correlate the ferrous RR data with structural considerations on the QS ferric heme. Nevertheless, it should be emphasized that the observation of a ν(Fe-Im) stretch at 237 cm^{-1}, while reduced with respect to CCP and HRP-C, still reflects a proximal ligand with strong imidazolate character that generates a strong ligand field. The ν(Fe-Im) frequency in the absence of H-bonding is expected to be ~200 cm^{-1} (Smulevich et al., 1988).

At this point it is worth mentioning an interesting proposal that has been made recently with regard to the origin of the QS state (Cheng et al., 1997). This suggests that saddle-shaped deformation and not a weak axial field, as previously proposed (Scheidt and Reed, 1981), may be the prime factor governing the occurrence of the quantum mixed spin state in heme proteins. Interestingly, the structural data of BP 1 show such a saddle-shaped deformation, as previously observed for various cytochromes *c′* (Finzel et al., 1985; Yasui et al., 1992; Ren et al., 1993). The possible influence of heme deformation in the generation of the QS heme state will be developed further in the following section. However, it should to pointed out here that of the four available crystal structures of cytochromes *c′*, the saddling deformation is small (only −0.41 to −0.53 Å), and the saddling is the dominant deformation for only *Rhodopirillum molischianum*. For *Chromatium vinosum* cytochrome *c′*, the saddling is even smaller (−0.16 to −0.35 Å). Thus it is unlikely that such a small saddling deformation alone would result in the QS spin state, because saddling of this magnitude occurs in many heme proteins.

Low-temperature studies provide an opportunity to obtain information on the thermal equilibrium of the spin and coordination states of the heme. A detailed quantitative analysis of the BP 1 EPR spectra has not been possible with the currently available data; however, it is clear that QS heme states are present in both the pH 4.0 and 6.5 samples, but the proportion is much greater at pH 6.5. This is in complete agreement with the absorption and RR results, where the marked increase in the population of the QS heme spin state at low temperature with respect to room temperature is particularly evident. The transition to the QS heme form is, however, only complete at pH 6.5, 20 K.

An upshift of the BP 1 RR core size marker bands at 20 K by ~10 cm^{-1} is clearly seen by comparing Figs. 3 and 8. Smaller effects have been noted previously in other heme proteins (Smulevich et al., 1991; Feis et al., 1994) and attributed to a contraction of the heme core resulting from an increase in the protein packing forces at low temperature. It is possible that in this case part of the increase in band frequencies at low temperature results from a greater proportion of the IS state in the QS state, because of an increased separation of the $d_{x^2-y^2}$ and d_{z^2} orbitals. It could

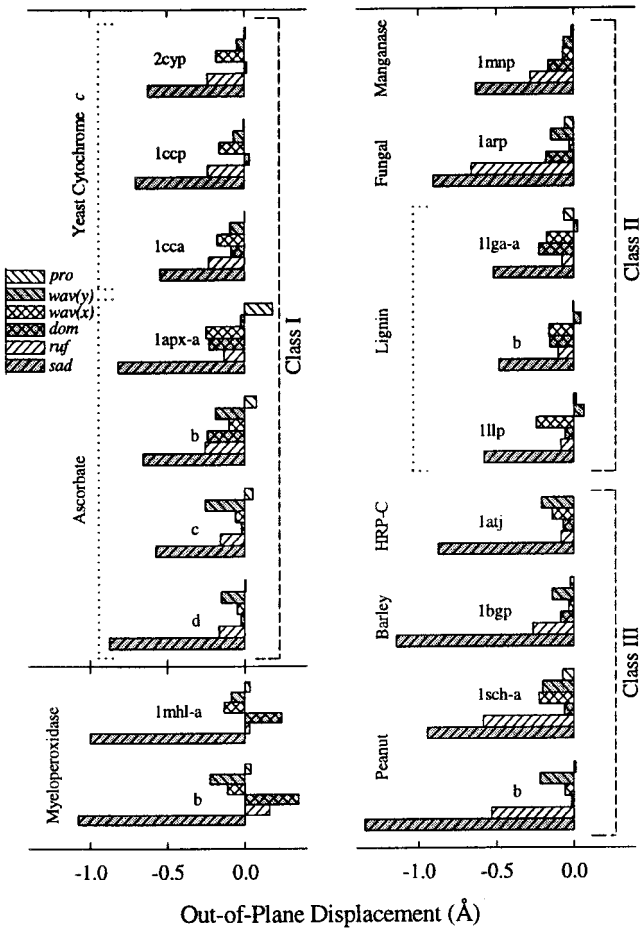

FIGURE 10 Out-of-plane displacements (minimal basis) for the heme groups in the x-ray crystal structures of peroxidases from different classes.

also be a result of a temperature dependent change in heme out-of-plane conformation.

Heme out-of-plane distortion

To investigate the possible importance of out-of-plane distortion in bringing about the QS state, we examine the available structural data for the peroxidases in detail, using NSD analysis. The out-of-plane distortions of the hemes for many types of heme proteins are conserved across the natural variation in their amino acid sequence. This is the case for mitochondrial cytochromes *c*, the tetraheme cytochromes c_3 (except for heme 4), and several other hemoproteins (Hobbs and Shelnutt, 1995; Shelnutt et al., 1998; Ma et al., 1998a), including the peroxidases. For the *c*-type cytochromes especially, this is not surprising, because the short covalently linked segment of the protein has been found to cause the large, primarily ruffled distortion (Ma et al., 1998b). Natural sequence variation rarely occurs in this short segment, so there is little structural variation for the mitochondrial cytochromes. Furthermore, the moderate distortion (~1 Å) observed for some cytochromes can be rationalized because the strong covalent attachments through the cysteine residues provide a means by which the protein can exert the strong forces necessary to significantly influence the heme conformation.

When the hemes of the peroxidases were investigated using NSD, we were surprised to find that the peroxidases also exhibit a conserved out-of-plane distortion as large as or larger than that of the cytochromes with covalent attachments at the heme periphery. Moreover, the mainly saddled deformation of the peroxidase heme is conserved for all of the peroxidase x-ray structures (with the exception of some prostaglandin H synthases). A strong negative-saddling feature is common to all of the peroxidase hemes, as is apparent from Fig. 10, irrespective of the class to which the peroxidase belongs. This saddling also occurs for myeloperoxidase, which, however, does not belong to the plant peroxidase superfamily. Its heme is covalently attached to the protein at several points, but the x-ray structure reveals weakly coordinated water molecules at 3.04 and 3.08 Å from the iron atom (Fenna et al., 1995), and the EPR is characteristic of HS heme (Hori et al., 1994). Saddling is not the predominant heme deformation for the x-ray structures of prostaglandin H synthases. However, all of the prostaglandin H synthase structures are at 3.5 Å or greater resolution. In addition, prostaglandin synthase has both peroxidase and cyclooxygenase active sites in the same protein.

In the absence of covalent linkage between the heme and the protein for peroxidases, the distortion must arise from the totality of the van der Waals contacts, the hydrogen bonding to the propionates, and the interactions with the axial ligand. It is not clear at present how the protein sequence can vary significantly (>80%) and still maintain the large saddling deformation. However, Fig. 10 shows considerable variation in the degree of saddling (0.5 to 1.5 Å). Similarly, there is variation in the contributions from other deformation types. In particular, the ruffling varies from −0.6 to 0.2 Å. There is variation among the peroxidases in the other deformation components (doming, waving [*x* and *y*]). These are typically small deformations, but usually with a negative sign. Myeloperoxidase is an exception to the latter, however, partly because the heme is inserted in the opposite sense with respect to the histidine ligand.

There is some information about the importance of particular residues that are in van der Waals contact with the heme that is contained in the NSD results for the x-ray structures of the cytochrome *c* peroxidase mutants. The NSD data for about half of the mutants are shown in Fig. 11. First notice that none of the mutations result in a heme without saddling as the major component of the distortion; only one mutant has significantly less saddling than the average of −0.6 Å noted for the rest of the CCP mutants and wild-type proteins. Nevertheless, the mutations do have significant influence on the heme nonplanarity in some cases. In particular, mutations occurring at W191 apparently increase the ruffling deformation. The closest contact between W191 and the heme is at a *meso*-carbon. Apparently, replacement of the large tryptophan residue with a smaller

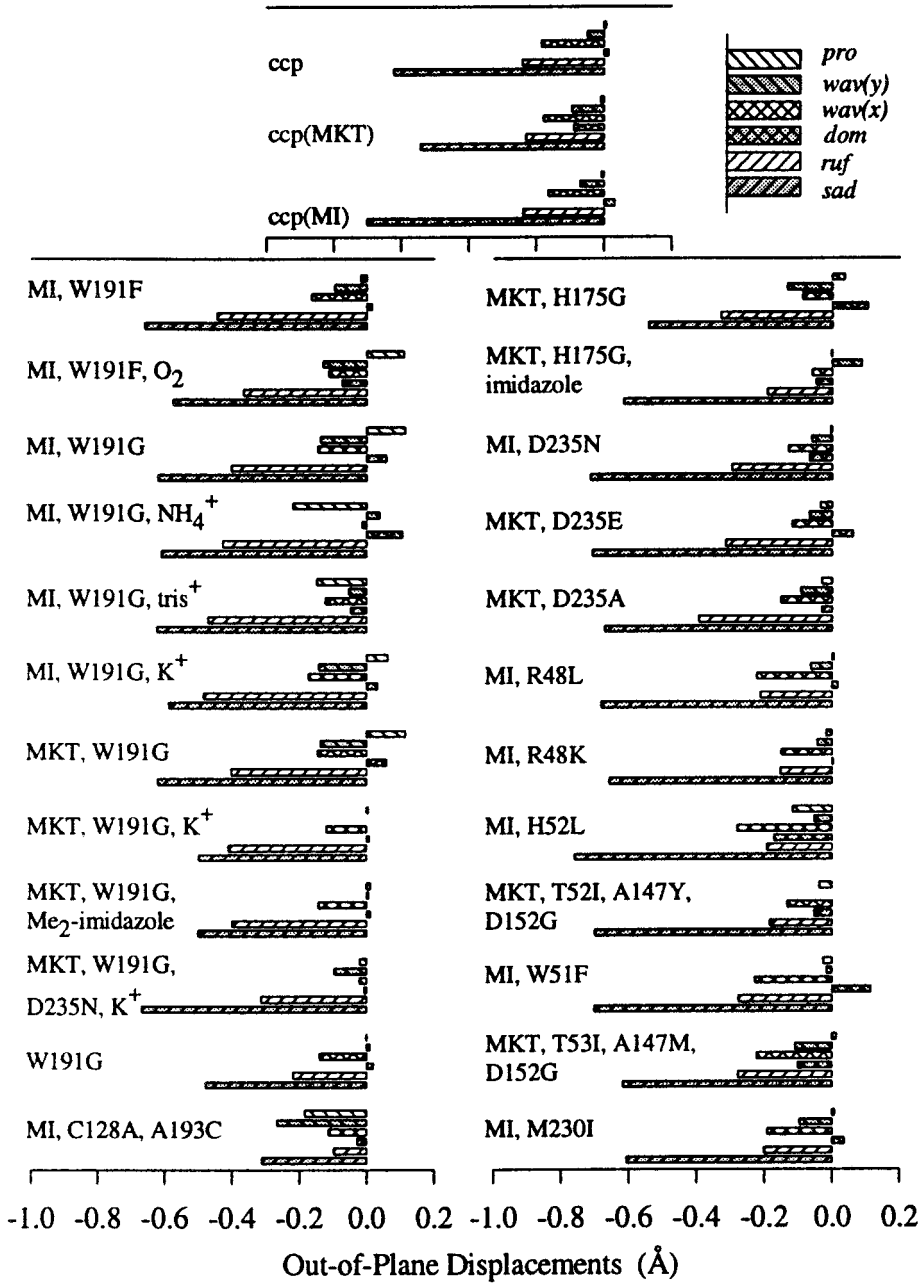

FIGURE 11 Out-of-plane displacements (minimal basis) for the heme groups in the x-ray crystal structures of yeast cytochrome c peroxidase and its mutants.

one in these so-called cavity mutants removes this close heme contact point. The result is that the *meso*-carbon of the heme can move out of the plane, and this must happen if the heme is to ruffle. Accordingly, most of the cavity mutants show a significant increase in the ruffling from −0.25 Å for the wild type to about −0.4 Å for the W191 mutants.

For the present work, the important question is whether the x-ray data support the proposal that saddling causes the QS state for the class III peroxidases. Anticipating the fact that saddling alone probably does not account for the QS state, we have investigated saddling in conjunction with other structural parameters. For example, Fig. 12 (*left*) shows a plot of the saddling deformation versus the displacement of the iron atom from the mean plane. Displacement of the iron from the plane was proposed earlier as the controlling factor in determining the content of the intermediate spin state for the cytochromes *c′*. Although the class III peroxidases tend to be more saddled than class I and class II peroxidases, it is apparent that there is no clear separation of the class III peroxidases from the others for these two structural parameters, individually or in combination. One might argue, however, that there are different trends in the data when they are plotted this way. Nevertheless, we must conclude that saddling alone or in combination with Fe displacement may not be sufficient to cause the QS state. However, because saddling is present in all cases of QS found so far, it may be necessary for forming the QS state.

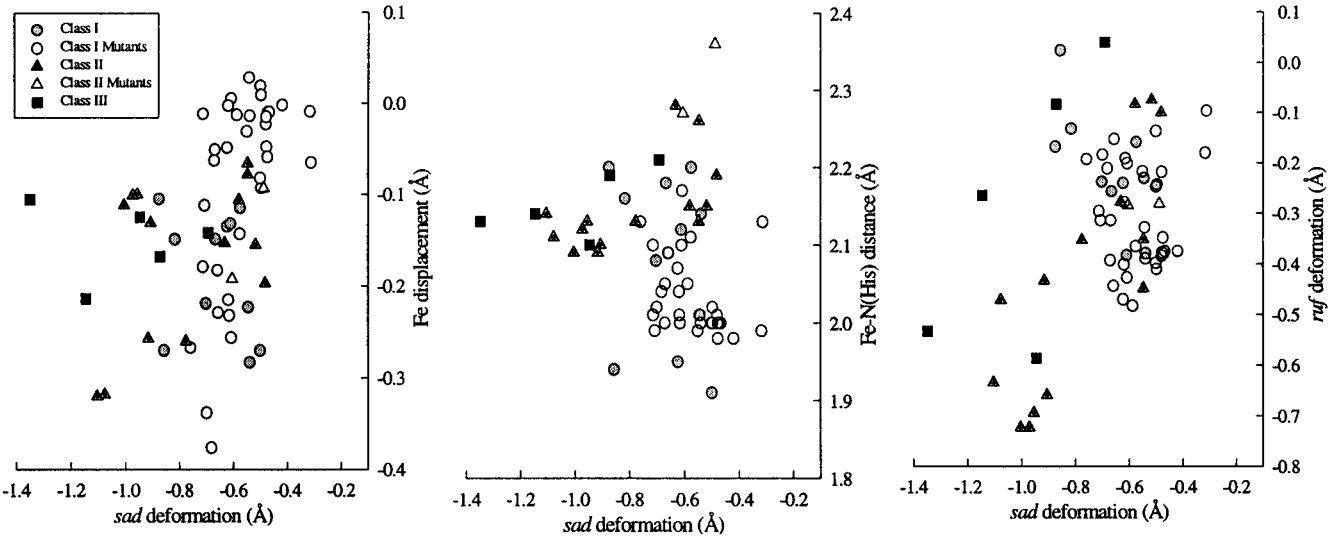

FIGURE 12 Relationships between the *sad* deformation of the heme group of peroxidases from the three classes and (*left*) the iron out-of-plane displacement, (*middle*) the Fe-N (imidazole) distance, and (*right*) the *ruf* deformation.

Other possible factors that might influence the spin state are the geometry of the histidine axial ligand, hydrogen bonding to imidazole, the presence of a sixth ligand, and other heme deformations. These structural parameters are listed in Table 2 for all of the available crystal structures. Fe out-of-plane displacement, alone or with saddling, clearly does not differentiate the class III peroxidases (Fig. 12, *left*). Similarly, plots of total out-of-plane distortion against the Fe-N(pyrrole) distance show no clear demarcation between the proteins of different classes. However, this plot (not shown) does show that as the distortion increases, the Fe-N bond length decreases until the optimum Fe(III)-N bond length in the porphyrin is reached (~1.975 Å). As the total distortion continues to increase beyond ~0.8 Å, only a slight further decrease in Fe-N distance is observed. This is consistent with model compound studies for which compression of the metal-N bond beyond the optimum distance is difficult (Shelnutt et al., 1991; Sparks et al., 1993).

A clear demarcation between the class I, II, and III proteins does not exist for any of the parameters investigated to date. Fig. 12 (*middle*) shows the plot of the Fe-N(imidazole) distance versus the saddling deformation, and Fig. 12 (*right*) that of heme saddling versus ruffling. We see that the class III proteins tend to be less ruffled for the degree of saddling they exhibit. Thus some competition between these deformations may play a role.

Other structural relationships are found between the coordination geometry and that of the macrocycle. For example, a weak relationship exists between the small doming of the heme and the iron displacement from the mean plane (Table 2). The relationship is clearest for the class II proteins. For native class I peroxidases, the doming deformations are randomly scattered, mostly between −0.1 and +0.1 Å and, including mutant proteins, between −0.2 and +0.2 Å. The corresponding Fe displacements are scattered between −0.4 and +0.1 Å (−0.3 and −0.1 for the native enzymes). Similarly, Fe displacements for native class III proteins are between −0.3 and −0.1 Å, and a negative doming may be favored. In contrast, for the class II proteins, Fe out-of-plane displacement is correlated with a doming, with the doming becoming as large as −0.4 Å for Fe displacements of −0.3 Å.

CONCLUSIONS

A characterization of BP 1 by electronic absorption, RR, and EPR spectroscopy at room and low temperatures has shown that it is a mixture of HS states and the uncommon QS heme state. The relative populations of the states are dependent on pH and temperature, but the QS heme form, which is always the dominant species, is present as a unique state at pH 6.5 at 20 K, whereas the HS form is maximized at pH 3.3 at room temperature. The vinyl stretching modes are split in the RR spectra, indicating that the two vinyl groups have different degrees of conjugation with the porphyrin, consistent with other peroxidases of class III.

The apparent limitation of the QS state to class III peroxidases and the importance of heme saddling in generating the QS state have been discussed on the basis of all of the structural data currently available for the peroxidases. The generalization that only class III proteins are QS might be not be valid. However, of all of the proteins reported in Table 2, only a few have not had their spin state characterized. All have been found to have either a LS or HS heme spin state, apart from those of class III. Unfortunately, only three x-ray structures of class III proteins are available. On the other hand, if it does turn out that the QS only occurs for class III peroxidases and not for class I and II proteins, it is difficult to justify the conclusion that it is a consequence of

saddling or a weak ligand field alone. Other structural factors must be considered to account for the unusual spin-state properties of the class III peroxidases. The class III peroxidases diverge from both class I and II in two distinct ways: a unique loop containing helices F′ and F″ linked by a disulfide bridge, which is located between helices F (containing the proximal histidine) and G, and a short disulfide loop containing only four residues penultimate to the distal histidine.

We are grateful to Prof. R. C. Bray for providing facilities to record the EPR spectra, Prof. P. Lattanzi and Dr. C. Mainero for access to the micro-Raman instrument, and Dr. F. Neri (Università di Firenze) for skilled assistance in preparing some of the enzyme samples.

This work was supported by grants from the Italian Consiglio Nazionale delle Ricerche (CNR) and Ministero della Università e Ricerca Scientifica e Tecnologica (MURST ex 60% to MPM and Cofin. MURST97 CFSIB to GS), the University of Copenhagen (07-2236-57/93) and the Danish Research Academy (S940139) (to CBS), and the EC Human Capital and Mobility Programme (ERB CHRX-CT92-0012-130 to GS and KGW). BDH is funded by a fellowship from the EC as part of the above program. Sandia is a multiprogram laboratory operated by Sandia Corporation, a Lockheed Martin Company, for the U.S. Department of Energy under contract DE-AC04-94AL85000.

REFERENCES

Abola, E. E., F. C. Bernstein, S. H. Bryant, T. F. Koetzle, and J. Weng. 1987. Crystallographic Databases—Information Content, Software Systems, Scientific Applications. F. H. Allen, G. Bergerhoff, and R. Sievers, editors. Data Commission of the International Union of Crystallography, Bonn, Cambridge, and Chester. 107–132.

Abola, E. E., J. L. Sussman, J. Prilusky, and N. O. Manning. 1997. Methods in Enzymology. C. W. Carter, Jr., and R. M. Sweet, editors. Academic Press, San Diego. 556–571.

Blumberg, W. E., J. Peisach, B. A. Wittenberg, and J. B. Wittenberg. 1968. The electronic structure of protoheme proteins. *J. Biol. Chem.* 243: 1854–1862.

Cheng, R.-J., P.-Y. Chen, P.-R. Gau, C.-C. Chen, and S.-M. Peng. 1997. Control of spin state by ring conformation of iron(III) porphyrins. A novel model for the quantum-mixed intermediate spin state of ferric cytochrome c′ from photosynthetic bacteria. *J. Am. Chem. Soc.* 119: 2563–2569.

Choi, S., T. G. Spiro, K. C. Langry, K. M. Smith, D. L. Budd, and G. N. La Mar. 1982. Structural correlations and vinyl influences in the resonance Raman spectra of protoheme complexes and proteins. *J. Am. Chem. Soc.* 104:4345–4351.

Conroy, C. W., P. Tyma, P. H. Daum, and J. E. Erman. 1978. Oxidation-reduction potential measurements of cytochrome c peroxidase and pH dependent spectral transitions in the ferrous enzyme. *Biochim. Biophys. Acta.* 537:62–69.

deRopp, J. S., P. Mandal, S. L. Brauer, and G. N. La Mar. 1997. Solution NMR study of the electronic and molecular structure of the heme cavity in high-spin, resting state horseradish peroxidase. *J. Am. Chem. Soc.* 119:4732–4739.

Dunford, H. B. 1991. Horseradish peroxidase: structure and kinetic properties. *In* Peroxidases in Chemistry and Biology. J. Everse, K. E. Everse, and M. B. Grisham, editors. CRC Press, Boston. 1–24.

Dunford, H. B., and J. S. Stillman. 1976. On the function and mechanism of action of peroxidases. *Coord. Chem. Rev.* 19:187–251.

Feis, A., B. D. Howes, C. Indiani, and G. Smulevich. 1998. Resonance Raman and electronic absorption spectra of horseradish peroxidase isozyme A2: evidence for a quantum-mixed spin species. *J. Raman Spectrosc.* 29:933–938.

Feis, A., M. P. Marzocchi, M. Paoli, and G. Smulevich. 1994. Spin state and axial ligand bonding in the hydroxide complexes of metmyoglobin, methemoglobin, and horseradish peroxidase at room and low temperatures. *Biochemistry.* 33:4577–4583.

Fenna, R. E., J. Zeng, and C. A. Davey. 1995. Structure of the green heme in myeloperoxidase. *Arch. Biochem. Biophys.* 316:653–656.

Finzel, B. C., P. C. Weber, K. D. Hardman, and F. R. Salemme. 1985. Structure of ferricytochrome c′ from *Rhodospirillum molischianum* at 1.67 Å resolution. *J. Mol. Biol.* 186:627–642.

Fujii, S., T. Yoshimura, H. Kamada, K. Yamaguchi, S. Suzuki, S. Shidara, and S. Takakuwa. 1995. Electron paramagnetic resonance studies of ferric cytochrome c′ from photosynthetic bacteria. *Biochim. Biophys. Acta.* 1251:161–169.

Gajhede, M., D. J. Schuller, A. Henriksen, A. T. Smith, and T. L. Poulos. 1997. Crystal structure of horseradish peroxidase C at 2.15 Å resolution. *Nature Struct. Biol.* 4:1032–1038.

Henriksen, A., K. G. Welinder, and M. Gajhede. 1998. Structure of barley grain peroxidase refined at 1.9 Å resolution. *J. Biol. Chem.* 273: 2241–2248.

Hobbs, J. D., and J. A. Shelnutt. 1995. Conserved nonplanar heme distortions in cytochrome c. *J. Protein Chem.* 14:19–25.

Hori, H., R. E. Fenna, S. Kimura, and M. Ikeda-Saito. 1994. Aromatic substrate molecules bind at the distal heme pocket of myeloperoxidase. *J. Biol. Chem.* 269:8388–8392.

Jentzen, W., J.-G. Ma, and J. A. Shelnutt. 1998. Conservation of the conformation of the porphyrin macrocycle in hemoproteins. *Biophys. J.* 74:753–763.

Jentzen, W., X. Z. Song, and J. A. Shelnutt. 1997. Structural characterization of synthetic and protein-bound porphyrins in terms of the lowest-frequency normal coordinates of the macrocycle. *J. Phys. Chem. B.* 101:1684–1699.

Kalsbeck, W. A., A. Ghosh, R. K. Pandey, K. M. Smith, and D. F. Bocian. 1995. Determinants of the vinyl stretching frequency in protoporphyrins. Implications for cofactor-protein interactions in heme proteins. *J. Am. Chem. Soc.* 117:10959–10968.

Keilin, D., and E. F. Hartree. 1951. Purification of horseradish peroxidase and comparison of its properties with those of catalase and methaemoglobin. *Biochem. J.* 49:88–101.

Leigh, J. S., M. M. Maltempo, P.-I. Ohlsson, and K.-G. Paul. 1975. Optical, NMR and EPR properties of horseradish peroxidase and its donor complexes. *FEBS Lett.* 51:304–308.

Ma, J.-G., M. Laberge, X.-Z. Song, W. Jentzen, S.-L. Jia, J. Zhang, J. M. Vanderkooi, and J. A. Shelnutt. 1998a. Protein-induced changes in nonplanarity of the porphyrin in nickel cytochrome c probed by resonance Raman spectroscopy. *Biochemistry.* 37:5118–5128.

Ma, J.-G., J. Zhang, R. Franco, S.-L. Jia, I. Moura, J. J. G. Moura, P. M. H. Kroneck, and J. A. Shelnutt. 1998b. The structural origin of nonplanar heme distortions in tetraheme ferricytochromes c_3. *Biochemistry.* 37: 12431–12442.

Maltempo, M. M. 1976. Visible absorption spectra of quantum mixed-spin ferric heme proteins. *Biochim. Biophys. Acta.* 434:513–518.

Maltempo, M. M., T. H. Moss, and M. A. Cusanovich. 1974. Magnetic studies on the changes in the iron environment in *Chromatium* ferricytochrome c′. *Biochim. Biophys. Acta.* 342:290–305.

Maltempo, M. M., P. I. Ohlsson, K. G. Paul, L. Petersson, and A. Ehrenberg. 1979. Electron paramagnetic resonance analyses of horseradish peroxidase in situ and after purification. *Biochemistry.* 18:2935–2941.

Nissum, M., A. Feis, and G. Smulevich. 1998a. Characterization of soybean seed coat peroxidase: resonance Raman evidence for a structure-based classification of plant peroxidases. *Biospectroscopy.* 4:355–364.

Nissum, M., F. Neri, D. Mandelman, T. L. Poulos, and G. Smulevich. 1998b. Spectroscopic characterization of recombinant pea cytosolic pea cytosolic ascorbate peroxidase: similarities and differences with cytochrome c peroxidase. *Biochemistry.* 37:8080–8087.

Othman, S., P. Richard, A. Vermeglio, and A. Desbois. 1996. Evidence for a proximal histidine-protein interaction in the structure of cytochromes c′ in solution: a resonance Raman study. *Biochemistry.* 35:9224–9234.

Rasmussen, C. B., M. Bakovic, H. B. Dunford, and K. G. Welinder. 1993a. Reaction kinetics of barley peroxidase. *In* Plant Peroxidases: Biochemistry and Physiology. K. G. Welinder, C. Penel, and H. Greppin, editors. University of Geneva, Geneva, Switzerland. 155–158.

Rasmussen, C. B., M. Bakovic, K. G. Welinder, and H. B. Dunford. 1993b. Unique reaction of a barley peroxidase with hydrogen peroxidase. *FEBS Lett.* 321:102–105.

Rasmussen, C. B., A. Henriksen, A. K. Abelskov, R. B. Jensen, S. K. Rasmussen, J. Hejgaard, and K. G. Welinder. 1997. Purification, characterization and stability of barley grain peroxidase BP 1, a new type of plant peroxidase. *Physiol. Plant.* 100:102–110.

Rasmussen, C. B., A. N. P. Hiner, A. T. Smith, and K. G. Welinder. 1998. Effect of calcium, other ions, and pH on the reactions of barley peroxidase with hydrogen peroxide and fluoride. *J. Biol. Chem.* 273: 2232–2240.

Ren, Z., T. Meyer, and E. McRee. 1993. Atomic structure of a cytochrome c′ with an unusual ligand-controlled dimer dissociation at 1.8 Å resolution. *J. Mol. Biol.* 234:433–445.

Scheidt, W. R., and C. A. Reed. 1981. Spin-state/stereochemical relationships in iron porphyrins: implications for the hemoproteins. *Chem. Rev.* 81:543–555.

Schonbaum, G. R. 1973. New complexes of peroxidases with hydroxamic acids, hydrazides, and amides. *J. Biol. Chem.* 248:502–511.

Schuller, D. J., N. Ban, R. B. van Huystee, A. McPherson, and T. L. Poulos. 1996. The crystal structure of peanut peroxidase. *Structure.* 4:311–321.

Shelnutt, J. A., C. J. Medforth, M. D. Berber, K. M. Barkigia, and K. M. Smith. 1991. Relationships between structural parameters and Raman frequencies for some planar and nonplanar nickel(II) porphyrins. *J. Am. Chem. Soc.* 113:4077–4087.

Shelnutt, J. A., X.-Z. Song, J.-G. Ma, S.-L. Jia, W. Jentzen, and C. J. Medforth. 1998. Nonplanar porphyrins and their significance in proteins. *Chem. Soc. Rev.* 27:31–41.

Smulevich, G. 1998. Understanding the heme cavity structure of peroxidases: comparison of electronic absorption and resonance Raman spectra with crystallographic results. *Biospectroscopy.* 4:S3–S17.

Smulevich, G., A. English, A. R. Mantini, and M. P. Marzocchi. 1991. Resonance Raman investigation of ferric iron in horseradish peroxidase and its aromatic donor complexes at room and low temperatures. *Biochemistry.* 30:772–779.

Smulevich, G., A. Feis, C. Focardi, and K. G. Welinder. 1994a. Resonance Raman study of the active site of *Coprinus cinereus* peroxidase. *Biochemistry.* 33:15425–15432.

Smulevich, G., A. Feis, C. Indiani, M. Becucci, and M. P. Marzocchi. 1999. Peroxidase-benzhydroxamic acid complexes: spectroscopic evidence that a Fe-H_2O distance of 2.6 Å can correspond to hexa-coordinate high-spin heme. *J. Biol. Inorg. Chem*. 4:39–47.

Smulevich, G., S. Hu, K. R. Rodgers, D. B. Goodin, K. M. Smith, and T. G. Spiro. 1996. Heme-protein interactions in cytochrome c peroxidase revealed by site-directed mutagenesis and resonance Raman spectra of isotopically labeled hemes. *Biospectroscopy.* 2:365–376.

Smulevich, G., J. M. Mauro, L. A. Fishel, A. M. English, J. Kraut, and T. G. Spiro. 1988. Cytochrome c peroxidase mutant active site structures probed by resonance Raman and infrared signatures of the CO adducts. *Biochemistry.* 27:5486–5492.

Smulevich, G., M. Paoli, J. F. Burke, S. A. Sanders, R. N. F. Thorneley, and A. T. Smith. 1994b. Characterization of recombinant horseradish peroxidase C and three site-directed mutants, F41V, F41W, and R38K, by resonance Raman spectroscopy. *Biochemistry.* 33:7398–7407.

Sparks, L. D., C. J. Medforth, M. S. Park, J. R. Chamberlain, M. R. Ondrias, M. O. Senge, K. M. Smith, and J. A. Shelnutt. 1993. Metal dependence of the nonplanar distortion of octaalkyltetraphenylporphyrins. *J. Am. Chem. Soc.* 115:581–592.

Spiro, T. G., and X.-Y. Li. 1988. Resonance Raman spectroscopy of metalloporphyrins. *In* Biological Applications of Raman Spectroscopy. T. G. Spiro, editor. John Wiley and Sons, New York. 1–37.

Strekas, T. C., and T. G. Spiro. 1974. Resonance Raman evidence for anomalous heme structures in cytochrome c′ from *Rhodopseudomonas palustris. Biochim. Biophys. Acta.* 351:237–245.

Tamura, M. 1971. Optical and magnetic measurements of horseradish peroxidase. II. pH dependence of peroxidase. *Biochim. Biophys. Acta.* 243:249–258.

Tanaka, M., S. Nagano, K. Ishimori, and I. Morishima. 1997. Hydrogen bond network in the distal site of peroxidases: spectroscopic properties of Asn → Asp horseradish peroxidase mutant. *Biochemistry.* 36: 9791–9798.

Teraoka, J., and T. Kitagawa. 1980. Raman characterization of axial ligands for penta- and hexacoordinate ferric high and intermediate-spin (octaethylporphyrinato)iron(III) complexes. Elucidation of unusual resonance Raman spectra of cytochrome c′. *J. Phys. Chem.* 84:1928–1935.

Teraoka, J., and T. Kitagawa. 1981. Structural implications of the heme-linked ionization of horseradish peroxidase probed by the Fe-histidine stretching Raman line. *J. Biol. Chem.* 256:3969–3977.

Veitch, N. C. 1993. NMR studies of peroxidases. Thesis. Oxford University.

Wang, J., J. M. Mauro, S. L. Edwards, S. J. Oatley, L. A. Fishel, V. A. Ashford, N. Xuong, and J. Kraut. 1990. X-ray structures of recombinant yeast cytochrome c peroxidase and three heme-cleft mutants prepared by site-directed mutagenesis. *Biochemistry.* 29:7160–7173.

Welinder, K. G. 1992. Superfamily of plant, fungal and bacterial peroxidases. *Curr. Opin. Struct. Biol.* 2:388–394.

Yasui, M., S. Harada, Y. Kai, N. Kasai, M. Kusunoki, and Y. Matsuura. 1992. Three-dimensional structure of ferricytochrome c′ from *Rhodospirillum rubrum* at 2.8 Å resolution. *J. Biochem.* 111:317–324.